metals

MDPI

Article

Recycling Li-Ion Batteries via the Re-Synthesis Route: Improving the Process Sustainability by Using Lithium Iron Phosphate (LFP) Scraps as Reducing Agents in the Leaching Operation

Francesca Pagnanelli *, Pietro Altimari, Marco Colasanti, Jacopo Coletta, Ludovica D'Annibale, Alyssa Mancini, Olga Russina and Pier Giorgio Schiavi

Department of Chemistry, Sapienza University of Rome (IT), 00185 Rome, Italy;
pietro.altimari@uniroma1.it (P.A.); marco.colasanti@uniroma1.it (M.C.);
coletta.1671863@studenti.uniroma1.it (J.C.); ludovica.dannibale@uniroma1.it (L.D.);
alyssa.mancini@uniroma1.it (A.M.); olga.russina@uniroma1.it (O.R.); piergiorgio.schiavi@uniroma1.it (P.G.S.)
* Correspondence: francesca.pagnanelli@uniroma1.it

Abstract: The development of hydrometallurgical recycling processes for lithium-ion batteries is challenged by the heterogeneity of the electrode powders recovered from end-of-life batteries via physical methods. These electrode materials, known as black mass, vary in composition, containing differing amounts of nickel, manganese, and cobalt (NMC), as well as other chemicals, such as lithium iron phosphate (LFP). This study presents the results of the hydrometallurgical treatment of mixed NMC and LFP black masses aimed at creating flexible recycling processes. This approach leverages the reducing power of LFP to optimize the leach liquor composition for re-synthesizing NMC precursors. In particular, the leaching conditions were optimized based on the LFP content in the solid feed to maximize the extraction of key metals (Ni, Mn, Co, and Li). The leaching solid residue, graphite, was treated and characterized as a secondary raw material for new anode preparation. Iron phosphate was recovered by increasing the pH of the leach liquor, and the NMC precursors were obtained via coprecipitation. This process achieved a recycling rate of 51%, based on the black mass input and the mass of recovered elements in the output products. Additionally, substituting LFP scraps as the reducing agent in place of H_2O_2 reduced the recycling process's environmental impact by avoiding 1.7 tons of CO_2-equivalent emissions per ton of NMC black mass.

Keywords: black mass; LFP scraps; recycling; hydrometallurgy; re-synthesis; NMC precursors: graphite

Citation: Pagnanelli, F.; Altimari, P.; Colasanti, M.; Coletta, J.; D'Annibale, L.; Mancini, A.; Russina, O.; Schiavi, P.G. Recycling Li-Ion Batteries via the Re-Synthesis Route: Improving the Process Sustainability by Using Lithium Iron Phosphate (LFP) Scraps as Reducing Agents in the Leaching Operation. *Metals* **2024**, *14*, 1275. https://doi.org/10.3390/met14111275

Academic Editor: Petros E. Tsakiridis

Received: 28 September 2024
Revised: 3 November 2024
Accepted: 5 November 2024
Published: 9 November 2024

1. Introduction

Lithium-ion batteries are the preferred technology for applications in automobiles, portable electronic devices, and stationary renewable energy storage systems. Consequently, they play a crucial role in the energy transition and are expected to significantly impact the global market. Online market analyses report compound annual growth rates (CAGR) of 13–18% for the 2020–2030 period, with the market projected to reach USD 77 billion by 2030 [1,2]. The lithium-ion battery market is diverse in terms of the formats and chemical compositions, particularly regarding cathode materials. Cathodes can consist of monometallic oxides like LCO ($LiCoO_2$) and LMO ($LiMn_2O_4$), mixed oxides like NMC (nickel–manganese–cobalt oxides with various stoichiometric ratios such as 111) or NCA (nickel–cobalt–aluminum), and lithium iron phosphate (LFP) [3]. Each type has unique advantages and limitations related to its specific capacity, durability, and safety, leading to specialized applications. NMC is commonly used in portable electronics and electric vehicles, while LFP is used in public transportation and stationary energy storage systems [3].

The transition to renewable energy sources is expected to increase the consumption of non-renewable raw materials for energy production, storage, and distribution. To

align the green transition with sustainable development, more efficient use of these non-renewable mineral resources is essential. Recycling materials from end-of-life lithium-ion batteries is currently the primary strategy to reduce reliance on non-renewable resources by substituting them with secondary raw materials. This is particularly important given the emerging needs of the battery market and the entry of new European players, who aim to use recycled materials to meet production demands.

An integrated recycling and electrode production approach would ideally combine end-of-life battery processing with the manufacturing of new electrode materials (cathodes and anodes) within a single plant. The re-synthesis-based hydrometallurgical recycling process, for instance, enables the recovery of graphite (from leaching residues) and produces cathodic material through coprecipitation on purified leachates, followed by lithiation and thermal activation [4,5]. Integrating recycling and synthesis reduces the process steps, minimizes downstream processing, and enhances sustainability. The variety of cathode materials often necessitates adjustments to the leaching solution for NMC precursor coprecipitation with varying compositions. This approach aligns with the new Battery Regulation [6], which mandates the minimum recycled material percentages in EU-manufactured batteries by 2030—12% for Co, 4% for Ni, and 4% for Li. Primary raw material salts can be added to leachates as needed to meet these requirements.

Hydrometallurgical recycling faces two main challenges: material heterogeneity and impurities in the black mass—a mixture of graphite, anodic carbon-based materials, and cathodic compounds recovered from spent lithium-ion batteries. Economic and safety considerations have driven the evolution of cathodic materials, resulting in diverse chemistries, primarily characterized by varying NMC stoichiometries (Ni, Mn, and Co molar ratios). Recent studies have highlighted the benefits of NMC-LFP cathode blending, which combines NMC's high density with LFP's thermal stability [7–11]. This trend reveals that sorting batteries before recycling cannot effectively address the chemical heterogeneity of electrode materials, as NMC-LFP blends cannot be separated efficiently.

The current literature has largely focused on the recycling of single-type black mass, optimizing the leaching and recovery conditions for NMC materials through first- and second-generation hydrometallurgical processes. The latter avoids salt separation and instead generates mixed NMC precursors through coprecipitation [12]. Physical processes that release battery components introduce metallic impurities (e.g., iron, aluminum, and copper) into the black mass, which must be removed before precursor coprecipitation to preserve the electrochemical performance. The literature suggests that cathodes can tolerate specific impurity levels (e.g., 0.2–3% for Al, 0.5% for Fe, and 2.5–6% for Cu) without compromising performance [13–18].

Regarding LFP recycling, the low intrinsic material value has led to direct regeneration processes that preserve its structure [19]. Selective leaching for lithium recovery has been proposed due to Li's relatively high value [20]. However, the economic viability of a hydrometallurgical process for low-value materials remains uncertain, especially given the trends in NMC-LFP blending. This blending underscores the need for recycling processes capable of simultaneously treating NMC and LFP black mass, which would offer environmental advantages.

Transition metal (TM) recycling from NMC materials is complex, as these metals are present in multiple oxidation states within black mass particles [21,22]. Research on NMC111 leaching reveals a staged process where lithium deintercalation initially releases electrons, reducing Ni, Co, and Mn, and partially leaching TMs (36% for Ni and Co, 40% for Mn, and 72% for Li) [23,24]. After 15–20 min, Mn extraction drops, with MnO_2 formation inhibiting Ni and Co extraction. Adding a reducing agent, like hydrogen peroxide, is often necessary to achieve full TM recovery. However, hydrogen peroxide's environmental impact due to hydrogen gas use and catalyst requirements has prompted studies of alternative, more eco-friendly reducing agents, such as organic acids and sugars [25].

More recently, studies have explored the simultaneous leaching of NMC and LFP black masses, often derived from unsorted batteries or inseparable NMC-LFP blends [26]. In

such cases, LFP contributes impurities, which can either be minimized by oxidizing iron to precipitate it as phosphate or removed during subsequent purification [27,28]. Some studies use LFP as a reagent, eliminating the need for hydrogen peroxide by dissolving LFP in a non-oxidizing environment to release Fe^{2+}, which aids in TM reduction [29,30]. For instance, leaching experiments with 2 M H_2SO_4 at 30 °C for 2 h reported high TM extractions (87.6% for Ni, 100% for Co, and 91.1% for Mn) by adding LFP as a reducing agent.

This work presents, for the first time, an integrated NMC-LFP recycling process without peroxide, from cryo-milling to cathode and anode production from oxalate precursors. While other studies have employed low levels of incidental LFP or used alternative leaching solutions (e.g., ferric salt solutions or hydrochloric acid) without re-synthesizing the precursors [26–33], this work utilizes LFP as a controlled reagent, demonstrating the viability of peroxide-free recycling for mixed NMC-LFP black masses.

2. Materials and Methods

2.1. Materials

The NMC black mass was provided by S.E.Val. (Colico, Italy) by performing cryo-mechanical treatment of EoL Li-ion batteries of the NMC type according to the optimized process route developed in the LIFEDRONE project [6]. The process included cryo-mechanical crushing, dry separation (sieving and magnetic separation) and a final bathing in water [34]. The cryo-mechanical section (400 kg/day potentiality) included a cryogenic pretreatment performed on the batteries in order to prevent explosions and control flame formation during crushing. Thermally stabilized batteries (−80 °C for 45 min using an N_2 liquid shower in a cabinet) were then crushed in a hammer mill with a 10 mm under-sieve. The crushed material was sieved (1 mm) and the over-sieve was separated by magnetic separation using a magnetic over-belt placed above the sieving belt. After this treatment, three fractions were collected: fine powder made up of electrode materials (NMC black mass), a coarse magnetic fraction made up of external steel cases, and a non-magnetic coarse fraction made of large fragments of collectors and separators of plastic and papers. Copper and aluminum fragments from the non-magnetic over-sieve fraction were separated by eddy currents. After separation, the three fractions (NMC black mass and coarse fractions) were washed in water to avoid flame formation due to solvents. The LFP black mass was made up of cathode scraps furnished by FAAM as manufacturing waste.

2.2. Characterization of NMC Black Mass and LFP Scraps

The chemical composition of the input solids was determined by mineralization of the solids in acid solution and successive analyses of the resulting solutions by an inductively coupled plasma–optical emission spectrophotometer (ICP-OES, Avio 220 Max, Perkin Elmer, MA, USA). Mineralization experiments were carried out by weighing 0.100 g of solid; these were placed in a 50 mL flask into which 4 mL of hydrochloric acid (37%ww, VWR Chemicals, Radnor, PA, USA) 4 mL of nitric acid (65%ww, VWR Chemicals, Radnor, PA, USA), and 2 mL of hydrogen peroxide solution (30%ww, Merck, Darmstadt, Germany) were added. The sample was subjected to magnetic stirring at a temperature of approximately 100 °C for 3 h. The mineralization operation just described was replicated to estimate the experimental error and sample variability (9 replicates for NMC black mass and 12 replicates for LFP scraps). Finally, the solutions were analyzed with ICP-OES, from which the different concentrations of the metals of interest were obtained. The limit of detection (LOD) was determined by taking the mean blank intensity, adding three times its standard deviation, and dividing it by the slope of the calibration curve specific to each metal analyzed. LOD (mg/L): Li 0.04, Ni 0.8, Co 0.0007, Cu 0.02, Mn 0.003, Fe 0.002, Al 0.003, P 0.02, V 0.04.

2.3. Leaching

Metal extraction from the NMC-LFP mixtures was performed considering different LFP fractions as the weight of LFP scraps over the total leached powder (10 g). In particular, the investigated LFP fractions were 0.34, 0.47, 0,51, and 0.58. Solids (NMC + LFP) were

leached in thermos-stated jacketed vessels under magnetic stirring with 1.5 M sulfuric acid (95% ww, VWR Chemicals, Radnor, PA, USA) and a 1/10 solid to liquid ratio (g/mL) at 60 °C for 3 h. For each LFP fraction level, 3 replicates were performed. After leaching, residual solids were separated by centrifugation and the liquids were analyzed by ICP-OES to determine the metal extraction yields. The NMC black mass was also subjected to acid leaching without any reducing agent (1.5 M H_2SO_4, 1/10 solid to liquid ratio, 60 °C for 3 h).

2.4. Leaching Residue Treatment for Graphite Regeneration

The solid residue of the leaching was subjected to a second leaching to eliminate the residual metal impurities (conditions of the leaching: 1.5 M H_2SO_4, 1/10 solid to liquid ratio, 60 °C for 3 h, under magnetic stirring) and to thermal treatment at 500 °C for 3 h (100 °C/min) in a muffle furnace (L3/11/B410, Nabertherm GmbH, Lilienthal, Germany). The chemical composition of the residues after the first and second leaching and after the thermal treatment was determined by the mineralization procedure and ICP-OES analyses as described before. Field emission scanning electron microscopy (SEM, Auriga, Zeiss, Oberkochen, Germany) was employed to characterize the morphology and size of the recovered materials. The crystal structure of the recovered graphite was evaluated by the X-ray diffraction patterns (XRD, D8 ADVANCE, Bruker, Billerica, MA, USA).

2.5. Precipitation for Iron Phosphate Recovery

The chemical precipitation of iron phosphate was performed by increasing the leach liquor pH up to 2.5 by adding NaOH (Emsure Supelco, Merck, Darmstadt, Germany) under magnetic stirring at room temperature for 1 h. The suspensions were then centrifuged for solid/liquid separation. The liquid samples were analyzed by ICP-OES for determination of the residual metal concentrations in the solutions and the solid samples were dried in an oven at a constant weight and then characterized by mineralization and ICP-OES for the metal content.

2.6. Coprecipitation for NMC Precursors Recovery

After the iron phosphate removal, purified leach liquor samples were added for synthetic salts of Ni and Co ($NiSO_4$ hexahydrate 98%, Thermo Scientific, Waltham, MA, USA; $CoSO_4$ heptahydrate, VWR Chemicals, Radnor, PA, USA), with Mn being the most abundant element. The salts were added in order to obtain the initial metal concentration of Ni, Co and Mn in solution with the desired molar ratio or stoichiometry. In particular, NMC precursors with stoichiometry 111 (1 mol of Ni, 1 mol of Mn and 1 mol of Co) and 811 (8 mol of Ni, 1 mol of Mn and 1 mol of Co) were synthetized by adding to the leach liquor a solution of oxalic acid with a 1.5 molar concentration prepared using oxalic acid (Anhydrous 98%, Thermo Scientific, MA, USA). Precursor synthesis was performed in jacketed reactors (Lenz Laborglas GmbH & Co. KG, Wertheim, Germany) (height: 12 cm, diameter: 4.8 cm, volume: 217 mL) at 60 °C using mechanical stirring (1000 rpm) for 3 h. The solids were then separated by centrifugation and analyzed by mineralization and ICP-OES analyses for the metal content. The residual metal concentration after precursor precipitation was determined by ICP-OES to assess the final concentration of this stream (residual leach liquor) that should be used for Li recovery (not performed in this work).

3. Results

3.1. Chemical Composition of NMC Black Mass and LFP Scraps

Different samples of NMC black mass and LFP scraps were characterized in order to assess the variability in the chemical composition due to both material heterogeneity and experimental errors in the mineralization procedure. In Figure 1, the box plots of the element content (mg/g) are reported for the different metals, evidencing the range of variability (as a quartile plot), data distribution (as a violin plot) and out-layers. It should be noted that in order to better visualize the variability of the metal content for each metal,

a unique y axis was not used and the range of variability for each metal was evidenced by the upper and lower values.

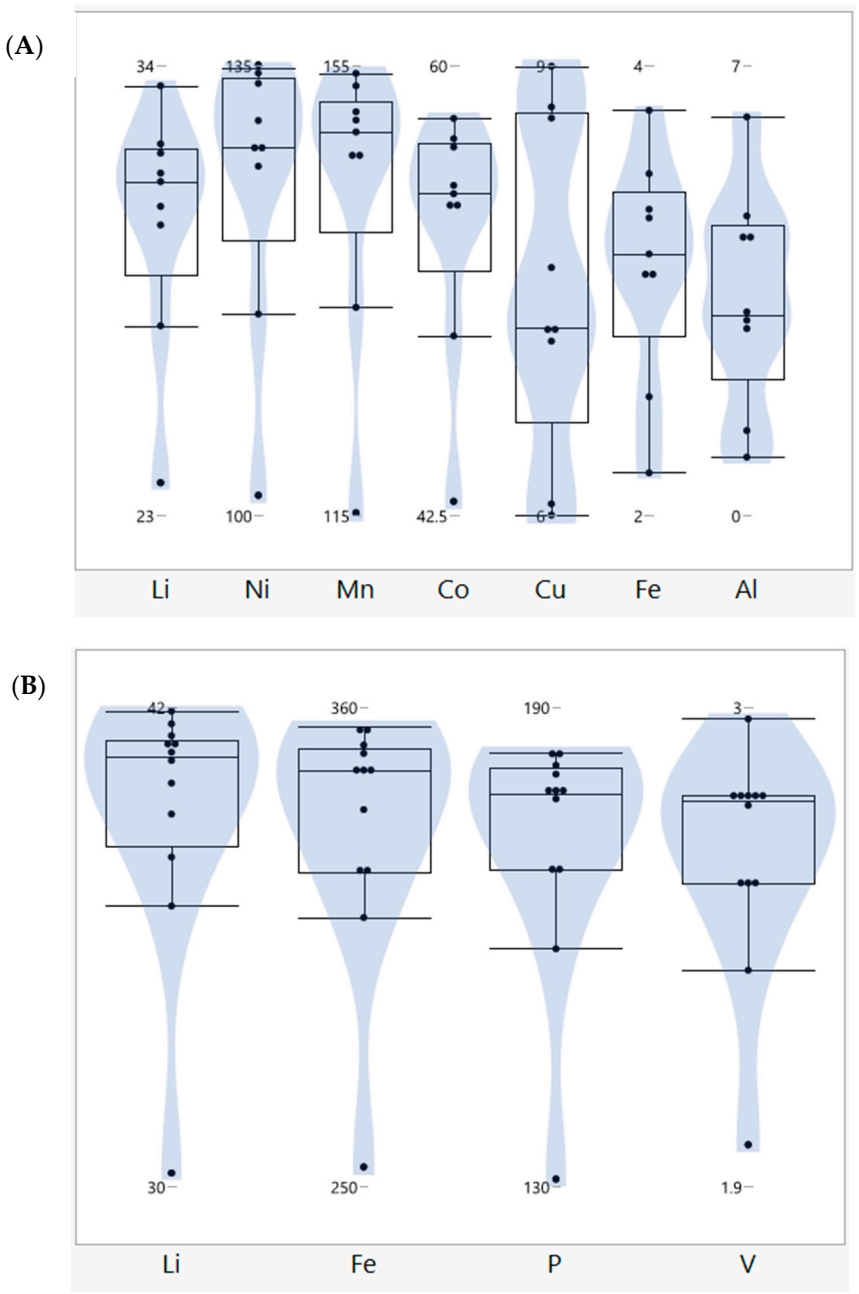

Figure 1. Box plots, violin plots and out-layers for the metal content (mg/g) in NMC black mass (**A**) and LFP scraps (**B**).

The mean chemical compositions of the NMC black mass and LFP scraps are then reported in Table 1 as mg/g with the margin of error as the estimated errors (95% confidence level). In the NMC black mass, the variability of the target metal contents (Li, Ni, Mn, Co) is quite low (margin of error < 7% of the mean), denoting that an adequate procedure was adopted in terms of the solid weight amount used as a representative of the black mass heterogeneity, number of replicates, and reproducible experimental protocol.

Table 1. Chemical composition (mg/g) of NMC black mass and LFP scraps: mean values ± margin of error (95%) (nd: not detected).

Metal	NMC (mg/g)	LFP (mg/g)
Li	30 ± 2	39 ± 2
Ni	128 ± 8	nd
Mn	140 ± 10	nd
Co	54 ± 4	nd
Cu	7.5 ± 0.8	nd
Al	3 ± 1	nd
Fe	3.1 ± 0.4	330 ± 20
V	nd	2.7 ± 0.2
P	nd	170 ± 10

As for the metal impurities, the margin of error accounts for a larger percent variation of the measured content (11–37%) and this could be due to the random presence of fragments of Cu, Al and Fe in the black mass. Indeed, the Fe, Al, and Cu impurities are due to the mechanical dismantling as small fragments of the internal layers and external case can pass the sieving phase, going in the under-sieve fraction with the black mass. The metal impurity contents evaluated as the %at. are 0.9%at. for Fe, 2.1%at. for Cu, and 2.0%at. for Al. These initial estimates evidenced the good quality of the black mass as these atomic percentages are in line with the values tested in doping experiments during the coprecipitation of precursors, as reported in the introduction. Nevertheless, the effect of the simultaneous presence of different metal impurities was not investigated yet. Then, even if the final content of impurities in the precursors is expected to be lower than that in the fed powders, the simultaneous presence of the different metal impurities in the final products could be negatively affected even at these low levels.

V is not present in the NMC cathodic materials, while P, which could be present as electrolyte residues ($LiPF_6$), is probably not detected due to the washing of the black mass after recovery at the dismantling plant.

The LFP scraps are more homogeneous in terms of the metal content (all margins of error are lower than 6% of the measured content) and do not present any impurity. Ni, Mn, and Co are not present in the LFP scraps according to the different cathodic composition of this type of battery, while Cu and Al are not present as LFP is a manufacturing scrap (a waste of the production lines of LFP batteries), so no dismantling of batteries was needed for the LFP scrap recovery.

3.2. Leaching Tests

The metal extraction (%) was determined for the different leaching conditions investigated, varying the LFP fraction in the feed, and is reported in Figure 2. Leaching of the NMC black mass in acid without a reducing agent was performed, confirming the incomplete dissolution of Ni (77%), Co (56%) and Mn (34%) in these conditions. The obtained results agree with a literature study investigating the mechanism of NMC dissolution in acid solutions without a reducing agent [35]. The addition of LFP scraps to NMC black mass greatly improved the extraction of the target metals. In Figure 2, the extraction yields (%) of Li, Ni, Mn, Co, Fe and P are reported for the different investigated levels of LFP fraction. Random errors due to both the heterogeneity of the powder and the multi-step experimental procedures of leaching and analytical determination of metals after dilution determined the variability of the data and registration of values over 100% extraction. In order to assess the significance of the effects, statistical regression analysis was then performed to isolate the effect of the random errors. All the metals present a similar trend, showing a significant effect of the LFP fraction, which could be adequately described by a second-grade polynomial. On the other hand, no significant effect of the LFP fraction was observed for Cu and Al impurities in the investigated range.

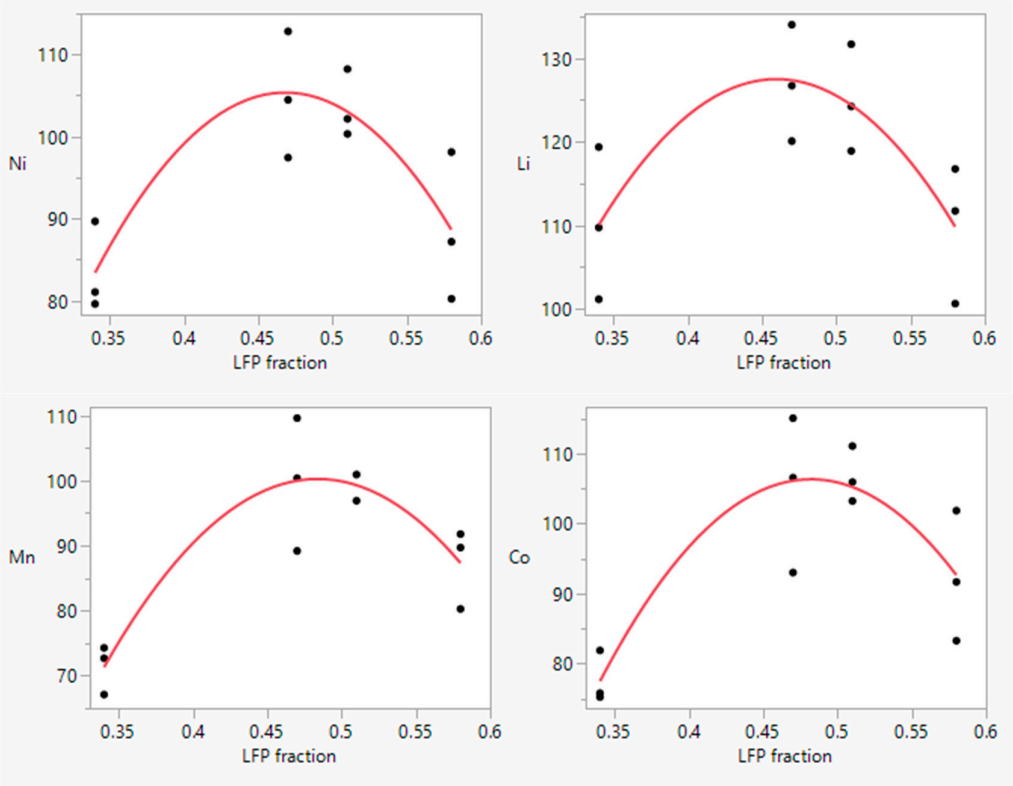

Figure 2. Metal extraction (%) as a function of the LFP fraction: experimental data and quadratic model.

In Table 2, the parameter values are reported for the metal extraction significantly affected (p value < 0.1) by the LFP fraction change according to the quadratic model in the coded variable with the following equation:

$$y = \beta_0 + \beta_1 \times x + \beta_2 \times (x - x_m)^2 \quad (1)$$

where y is the metal extraction yield (%), x is the LFP fraction, x_m is the mean of the investigated LFP fraction values, and β_0, β_1, and β_2 are the adjustable parameters regressed by the least squares method. The adequacy of the quadratic model is verified by the lack of fit test (LOF test), denoting for Li, Ni, Mn, Co, Fe, and P high p values, meaning that the null hypothesis concerning the model adequacy cannot be rejected.

Table 2. Quadratic models in coded variables representing the significant effect (p < 0.1) of the LFP fraction on the metal % extraction; p value for the lack of fit test (Prob > F).

Metal	β_0	β_1	β_2	LOF Test (Prob > F)
Li	144	−37	−1219	0.88
Ni	114	−18	−1338	0.86
Mn	88	24	−1398	0.91
Co	96	20	−1427	0.66
Fe	104	−9	−475	0.91
P	140	−886	−827	0.16

The experimental results and the statistical analysis evidenced that there is an optimum value of the LFP fraction, meaning that two opposite mechanisms are operating in terms of metal dissolution. In particular, for the lower range of tested LFP fraction (0.34–0.47), the increase in LFP determined an increase in metal dissolution, while in the upper range (0.51–0.58), increasing the LFP determined a significant reduction in Li, Ni, Mn, Co and P in the solution. The initial increase in metal dissolution can be explained considering

the active role of Fe(II) as a reducing agent in the dissolution of Mn and Co (and then Ni). On the other side, the decreasing dissolution can be explained by the reprecipitation of the dissolved metals, which in the presence of large concentration of phosphates can be reprecipitated.

Then, the antagonistic mechanisms could be metal dissolution promoted by an increasing Fe(II) concentration, and metal phosphate precipitation promoted by phosphate increased the concentration in the solution. Metal speciation confirmed this hypothesis in the case of Mn being insoluble as $MnHPO_4$. Further surface characterization of the solid residues after leaching is needed to confirm this theory.

According to the target of maximizing the extraction of all the metals, the optimum value of the LFP fraction evaluated by the quadratic models is LFP fraction = 0.4652. The effect of the variability of the LFP fraction and random errors can be simulated by Monte Carlo simulation, considering the LFP ratio as a random variable with a homogeneous distribution in the range optimum value ± 10% (0.42..0.51, corresponding to a 0.37 fraction of the initial range explored for the LFP fraction), adding a random error for each variable (estimated between 5 and 8% according to replicated tests) and assuming that the metal dissolution (Li, Ni, Mn, Co) should be larger than 95% to be process-specific. Under these assumptions, about the 60% of the results are in spec, denoting the need for fine control of the amount of LFP when used as a reactive in leaching.

3.3. Graphite Recovery

Graphite was recovered as a solid residue following the leaching of black mass. To remove the remaining metallic impurities, the recovered graphite underwent a second leaching process. As shown in Table 3, after this second leaching, the primary residual impurities are Ni (0.4 wt.%) and Fe (0.1 wt.%). Additionally, thermal regeneration was performed to remove the polymeric binder and conductive amorphous carbon present in the NMC black mass, along with metals and graphite. During this thermal treatment, a weight loss of 18 wt.% was observed, and the SEM images (Figure 3) confirm the removal of amorphous particles from the graphite surface. However, this weight reduction slightly concentrated the metallic impurities originally present in the graphite (II leaching—Table 3).

Table 3. Mean composition (mg/g) and margin of error for the graphite residues after the first leaching, after the second leaching, and after the thermal treatment (TT).

Treatment	Li	Ni	Mn	Co	Cu	Fe	Al	P
I leaching	10 ± 2	8 ± 1	1 ± 3	1.6 ± 0.9	0.2 ± 0.2	11 ± 8	0.7 ± 0.1	7 ± 3
II leaching	0.38 ± 0.02	4.4 ± 0.2	0.12 ± 0.03	0.67 ± 0.01	0.10 ± 0.02	1.4 ± 0.2	1 ± 1	0.48 ± 0.9
After TT	0.55 ± 0.02	5.28 ± 0.01	0.045 ± 0.007	0.77 ± 0.02	0.23 ± 0.04	2.7 ± 0.3	1.0 ± 0.1	1.56 ± 0.05

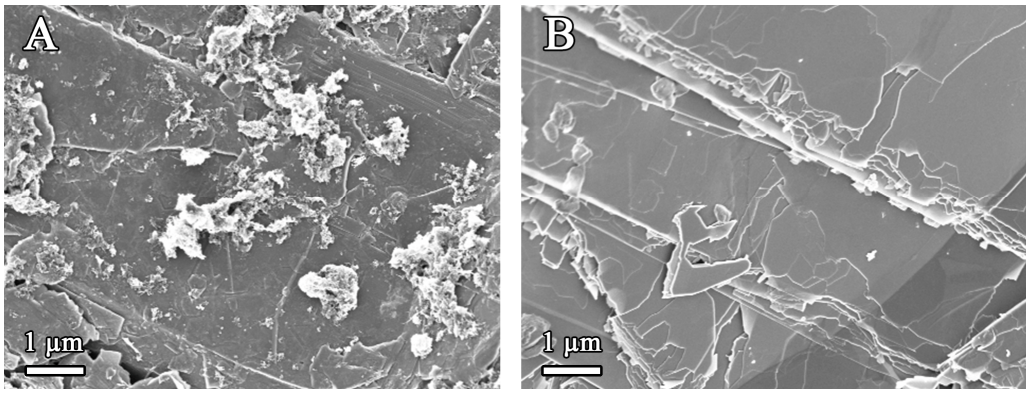

Figure 3. SEM images of graphite after the 2nd leaching (**A**) and after the thermal treatment (**B**).

The crystalline phase of the recovered material was identified using XRD powder diffraction. The XRD pattern of the recovered graphite is shown in Figure 4, alongside commercial graphite for comparison. Both samples display a sharp, narrow peak corresponding to the C (002) diffraction line typical of graphite's crystal structure. No differences between the two patterns were observed, and no additional phases were identified in the recovered graphite.

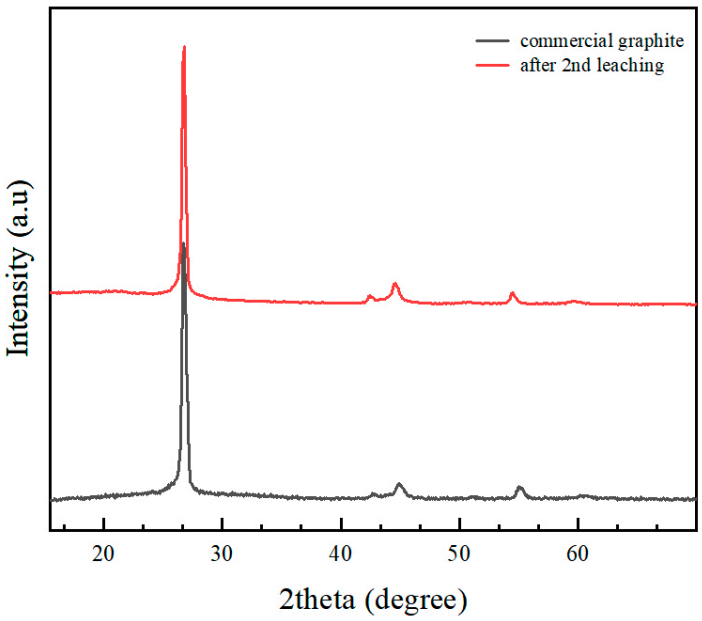

Figure 4. XRD diffractograms of commercial graphite and recovered graphite after the 2nd leaching.

3.4. Iron Phosphate Recovery

After leaching in optimal conditions (LFP fraction: 0.47–0.51), the leach liquor presents the average composition reported in Table 4. At pH 2.5, iron phosphate can be removed selectively by leach liquor, leaving the target metals (Ni, Mn, Co, Li) in the solution, as evidenced by the content of metals other than Fe and P in the recovered solid (Table 4).

Table 4. Mean composition and margin of error for the composition of the leach liquor (mg/L) obtained for the optimized LFP fractions and for the recovered solid $FePO_4$ (mg/g).

	Ni	Mn	Co	Li	Cu	Al	Fe	P
Leach liquor (mg/L)	6710 ± 520	7350 ± 630	2900 ± 240	4380 ± 220	510 ± 135	220 ± 60	16,440 ± 1100	8260 ± 930
$FePO_4$ (mg/g)	8 ± 2	8 ± 2	3.2 ± 0.6	4.6 ± 0.9	1.1 ± 0.3	4.3 ± 0.8	260 ± 25	125 ± 6

Considering the chemical composition, about 70% purity for $FePO_4$ (FP) is estimated, denoting the need for further optimization of this step, which can have a double aim: the refinement of the leach liquor before precursor precipitation, and the recovery of secondary raw materials.

3.5. NMC Precursors Recovery

After $FePO_4$ recovery, the leach liquor solution was purified from Fe and P (purified leach liquor). Before the precursor precipitation, the concentrations of Co and Ni in the leaching solution were adjusted to achieve the desired precursor stoichiometry (NMC 111 and NMC 811). In Table 5, the characterization of the NMC precursors is reported. For NMC111, the experimental formula $Ni_{0.38}Mn_{0.31}Co_{0.31}$ is obtained with an over-content of Ni. The impurities are 2%at. for both Cu and Al, while Fe and P are under the detection limits.

Table 5. Composition of the NMC111 and NMC8111 precursors (mg/g) (nd: not detectable).

Precursors (mg/g)	Ni	Mn	Co	Li	Cu	Al	Fe
NMC 111	126	94	103	0.97	8.0	3.0	nd
NMC 811	251 ± 5	14 ± 2	46 ± 1	0.86 ± 0.05	8 ± 1	5 ± 3	nd

For NMC811, the experimental formula is $Ni_{0.81}Mn_{0.04}Co_{0.15}$, with Mn under-stoichiometric and Co over-stoichiometric. The impurities are similar to the case of NMC111, that is, 2%at. for both Cu and Al, while Fe and P are under the detection limits.

3.6. Process Performances

The mass balance for the proposed process, which treats NMC black mass combined with LFP scraps, was developed based on experimental data collected at a lab scale for each operation described above: leaching, graphite regeneration, FP precipitation, and precursor precipitation. Experimental tests on lithium (Li) recovery from residual leach liquor (leach liquor after precursor precipitation) and production of NMC111 cathode materials have not yet been conducted. Thus, the yield for lithium recovery by precipitation as carbonate was set at 90% (based on results from similar systems) and the same precipitation was assumed for all the residual metals contained in the leach liquor solution following precursor recovery. Additionally, the metal quantities were assumed to remain constant during the thermal treatment stage for the final production of NMC cathode materials.

Table 6 shows the masses of the metals in the solid and liquid streams of the process at this stage of development, assuming a leaching feed consisting of 5 kg of NMC black mass and 5 kg of LFP scraps.

Table 6. Mass (g) of the input elements in the process flows using 5 kg of NMC and 5 kg of LFP.

Metal	Feed	Leach Liquor	Solid Residue I Leaching	FP	Purified Leach Liquor	Precursors	Residual Leach Liquor	Li Salt	NMC	Regenerated Graphite
Li	348	347	1	23	291	5	262	235	240	3
Ni	631	616	15	40	547	630	5	5	542	26
Mn	722	722	0	40	590	470	6	5	584	0
Co	269	266	3	16	237	515	2	2	235	4
Cu	38	37	1	6	30	40	2	1	41	1
Al	17	16	1	22	20	15	4	4	19	5
Fe	1680	1664	15	1300	124	0	40	36	36	14
P	866	854	12	625	56	0	56	50	50	8
V	13	13	0	0	0	0	0	0	0	0
C	2100	105	1995	0	0	0	0	0	0	1205
Tot	6684			2072					1748	1266

It is important to note that only the input element masses were considered in this mass balance. Oxygen, other added salts (such as oxalate or carbonate), and additional metal salts used to adjust the precursor stoichiometry (e.g., Ni and Co sulphates) were excluded. This approach was chosen to prevent artificially inflating the recycling rate of the process due to the addition of chemicals, in alignment with European legislation on battery recycling, as discussed in the conclusions section [6]. To better visualize the distribution of input metals across process streams, the data from Table 6 are illustrated in a Sankey diagram (Figure 5A), where the thickness of each flow through the various operations represents the mass it contains.

In the process that uses LFP scraps as a reducing agent, three primary products are recovered: FP (2.072 kg), NMC (1.748 kg), and regenerated anode material (1.266 kg), based on the total mass in these streams, as estimated in Table 6.

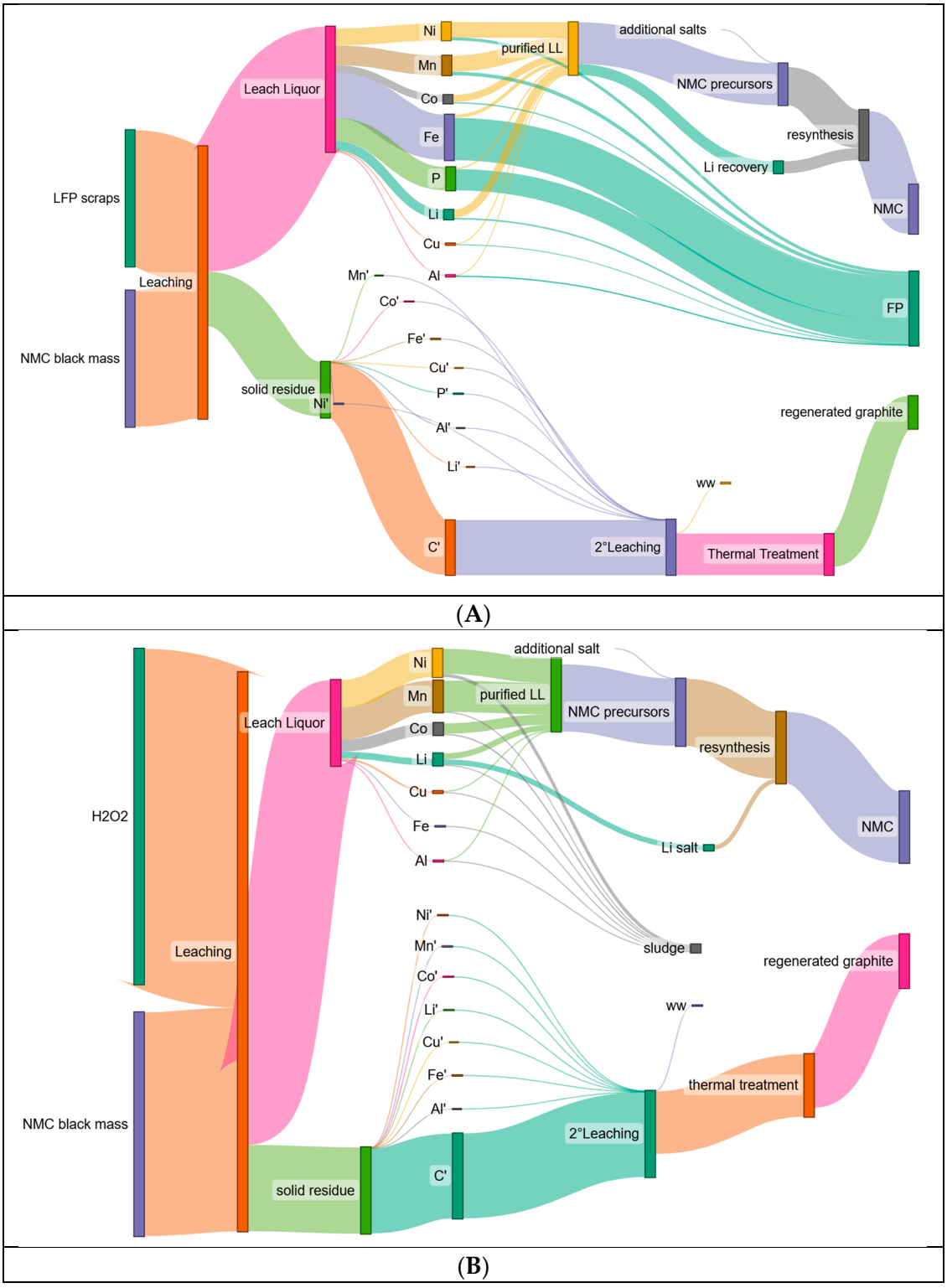

Figure 5. Sankey diagrams of the re-synthesis process for mixed NMC-LFP (**A**) and NMC-H_2O_2 (**B**): the masses are only those of the input elements in NMC black mass (Ni, Mn, Co, Li, Cu, Al, Fe, C), and LFP scraps (Li, Fe, P, V, C).

By summing the mass of the input elements in these products (5.087 kg) and dividing by the total input waste mass (10 kg), a recycling rate of 51% was calculated.

As a comparison to this process, a hydrometallurgical process involving hydrogen peroxide leaching and re-synthesis of precursors as oxalates can be considered (see Table 7

and Figure 5B). These are preliminary estimates, enabling an evaluation of the recovered product mass and calculation of the recycling rate for the hydrogen peroxide-based process. Notably, in this scenario, only NMC black mass (5 kg, as in the prior case) is used as the input waste. The resulting output products are NMC (1.631 kg) and regenerated graphite (1.162 kg). These product masses are similar or slightly lower than those in the NMC + LFP process. However, the recycling rate with hydrogen peroxide is approximately 56%, higher than that of the LFP process. This difference is solely due to the smaller input waste quantity, as the NMC + LFP process generates larger product masses starting from the same amount of NMC black mass. Thus, similar recycling rates can be achieved using LFP as a reducing agent, with three additional advantages: avoiding the environmental impacts associated with hydrogen peroxide, enabling LFP scrap treatment, and recovering additional secondary raw materials (FP). For impact mitigation, a preliminary estimate can be made based on the hydrogen peroxide dosage and its environmental impact, considering 30% *w*/*w* H_2O_2 solution (1.04 kg $CO_{2eq.}$/kg, from the Ecoinvent database). Considering the conventional process's use of hydrogen peroxide with a solid-to-liquid leaching ratio of 1:10, using LFP instead could potentially reduce the $CO_{2eq.}$ emissions by about 1.7 tons of $CO_{2eq.}$ per ton of NMC.

Table 7. Mass (g) of the input elements in the process flows using 5 kg of NMC and hydrogen peroxide as a reducing agent.

Metal	Feed	Leach Liquor	Solid Residue I Leaching	Metal Sludge	Purified Leach Liquor	Precursors	NMC	Regenerated Graphite
Li	151	150	2	18	132	13	120	1
Ni	631	624	6	67	557	552	557	7
Mn	722	715	7	13	702	695	701	0
Co	269	266	3	35	231	229	231	1
Cu	38	37	1	16	21	20	21	0
Al	17	17	0	15	2	2	2	2
Fe	16	8	7	8	0	0	0	2
C	2000		1900					1148
Tot	3843						1631	1162

Additional observations about the process performances can be made considering the recycling rate of the process in relation to the recycling targets set for lithium-ion batteries under the Battery Regulation, which will require 65% by 2025 and 70% by 2030 [6]. The explanatory notes on the calculation method for the recycling rate have not yet been issued. However, the previous regulations specified that only the elements entering with the batteries could be included in the product mass [35]. Thus, for example, oxygen was excluded from the product mass calculation unless it was used as an oxidant and certified as coming from the incoming waste by a third party.

The recycling rate calculation for the lithium-ion battery recycling process will always refer to the incoming batteries and not to the black mass. The first recycler handling the end-of-life battery will be responsible for achieving the recycling target if they do not also directly handle the black mass treatment. If the black mass is sold to another recycler, the first recycler must conduct operational due diligence to evaluate the company's operations, supply chain, and process efficiency, ensuring the overall target for the recycling rate. This raises the question of what minimum recycling rate a hydrometallurgical process using black mass as input must ensure. To answer this, it is necessary to assume a typical composition of the incoming battery and the recovery efficiencies for components that can be separated by physical operations along with the black mass (iron scrap, aluminum scrap, copper scrap, and electrolyte). According to the different types of batteries, the material composition can be quite variable [36]. Previous campaigns evidenced that by optimizing the physical pretreatment, it is possible to achieve complete recovery of black mass corresponding to 50% by weight of the battery [37]: then, 5 kg of NMC black mass corresponds to 10 kg of end-of-life batteries. As for copper, iron, and aluminum scraps, we can assume the % found during the demonstration campaign of the DRONE project [5],

denoting that the scraps of these metals are about 40% of batteries, with about 10% of electrolyte, plastic and paper. Assuming that the electrolyte is not recycled and there is a 90% recovery efficiency of Fe, Al, and Cu (for example, 4 × 0.9 = 3.6 kg out of 10 kg of batteries), the black mass recycling process must allow the recovery of a product mass of at least other 2.9 kg (6.5–3.6) to achieve a 65% recycling rate.

The NMC-H_2O_2 process ensures a recovery of 2.793 kg of products (1.631 kg NMC and 1.162 kg regenerated graphite), making it borderline for achieving the first 2025 target and unable to meet the 2030 target. However, the proposed process is simple, with nearly quantitative recovery yields in its stages. This contradiction between technological possibilities and regulatory targets will likely be resolved in the definition of the recycling rate formula, where elements like oxygen and carbon may not be counted in the incoming mass. In this case, excluding oxygen and carbon from the input mass, the NMC-H_2O_2 process would guarantee an adequate recycling rate to meet the 2030 target. Specifically, the input mass would be reduced from 10 kg of batteries to 5.843 kg of metals (4 kg from metal scraps of Fe of the outer casing, Cu, and Al of the current collectors; 1.843 kg from Ni, Co, Mn, Li of the black mass), from which 3.6 kg would be recovered, as previously assumed, in physical treatment and another 1.631 kg in the form of NMC cathodes, resulting in a recycling rate of 90% for the process (Table 8). In this case, the regenerated anode is not included among the output products in the recycling rate calculation.

Table 8. Mass (kg) of the input waste metals and output product metals for the process treating NMC with LFP scraps or NMC with H_2O_2 hydrogen peroxide.

	Input Metals (kg)			Output Metals (kg)			Recycling Rate (%)
Input Wastes	**Metal Scraps**	**NMC**	**LFP**	**Metals Scraps**	**NMC**	**FP**	
NMC LIB + LFP scraps	4	1.843	1.861	3.6	1.748	1.447	88
NMC LIB	4	1.843		3.6	1.631		90

In the case of the proposed innovative process, LFP scrap is also included in the recycling rate calculation as input. Assuming that oxygen and carbon are not counted in the incoming battery and applying the same approximations as above for the composition and recoveries in the pre-treatment phase, to treat the same quantity of 5 kg of NMC black mass, 5.843 kg of NMC battery metals would also enter, along with 1.861 kg of Fe and Li contained in 5 kg of LFP (assuming P is not counted like O and C, as it is not a metal). In this case, the products would include the metal masses in the NMC product (1.748 kg) and in the FP product (1.447 kg). The recycling rate for the NMC batteries and LFP scrap would thus be 88% = (3.6 + 1.748 + 1.447)/(4.0 + 1.843 + 1.861) × 100. Thus, from the perspective of the recycling rate calculated with respect to the incoming metals, the innovative process with LFP is equivalent to that with peroxide and both allow the achievement of the recycling rate established by the EU Battery Regulation for 2030 [6].

4. Conclusions

In this work, the technical feasibility of the LIB recycling route based on re-synthesis was assessed for NMC-LFP mixed black masses, proving the possibility of both using LFP as a reducing agent for NMC leaching and the selective recovery of FP from leach liquor before precursor re-synthesis.

The characterization of the mass flows was reported for the NMC-LFP feed in comparison with the NMC-fed process, denoting that the mass of products recovered from NMC black mass is almost the same. Nevertheless, treating NMC black mass and LFP manufacturing waste together can offer interesting advantages in terms of the environmental impacts, avoiding hydrogen peroxide usage and recovering FP, which could be hardly sustainable in a hydrometallurgical process dedicated to LFP batteries.

To conclude, using LFP scraps in the right dosage allowed the complete dissolution of the NMC target metals in the leaching, avoiding the use of hydrogen peroxide and thus reducing the environmental impacts of the process. Selective precipitation of FP allowed

the recovery of additional products without compromising the successive recovery of the NMC precursors.

Further investigations will address the electrochemical characterization of cathodic materials and regenerated graphite.

Author Contributions: F.P.: conceptualization, data curation, formal analysis, funding acquisition, methodology, project administration, resources, supervision, visualization, writing—original draft preparation, writing—review and editing. P.A.: conceptualization, formal analysis, writing—review and editing; P.G.S.: conceptualization, formal analysis, writing—review and editing; O.R.: investigation, formal analysis. M.C.: data curation, investigation, writing—review and editing. J.C.: data curation, investigation, writing—review and editing. L.D.: data curation, investigation, writing—review and editing. A.M.: data curation, investigation, writing—review and editing. All authors have read and agreed to the published version of the manuscript.

Funding: This work was co-funded by the EU LIFE+ program within the project "LIFE DRONE project: Direct pROduction of New Electrode materials from battery recycling" (ENV/IT/000520) www.lifedrone.eu (accessed on 3 November 2024).

Data Availability Statement: The original contributions presented in the study are included in the article, further inquiries can be directed to the corresponding author.

Conflicts of Interest: The authors declare no conflicts of interest.

References

1. Grand View Research. Available online: https://www.grandviewresearch.com/industry-analysis/advanced-battery-market (accessed on 3 November 2024).
2. Batteries News. n.d. Available online: https://batteriesnews.com/global-lithium-ion-battery-market-size-94-billion-2025 (accessed on 3 November 2024).
3. Kim, T.; Song, W.; Son, D.-Y.; Ono, L.K.; Qi, Y. Lithium-ion batteries: Outlook on present, future, and hybridized technologies. *J. Mater. Chem. A* **2019**, *7*, 2942–2964. [CrossRef]
4. Schiavi, P.G.; Branchi, M.; Casalese, E.; Altimari, P.; Navarra, M.A.; Pagnanelli, F. Resynthesis of NMC111 cathodic material from real waste lithium ion batteries. *Chem. Eng. Trans.* **2021**, *86*, 463–468. [CrossRef]
5. LIFEDRONE Project, LIFE DRONE Project: Direct PROduction of New Electrode Materials from Battery Recycling (ENV/IT/000520). n.d. Available online: www.lifedrone.eu (accessed on 5 November 2024).
6. Battery Regulation (EU) 2023, Regulation (EU) 2023/1542 of the European Parliament and of the Council of 12 July 2023 Concerning Batteries and Waste Batteries, Amending Directive 2008/98/EC and Regulation (EU) 2019/1020 and Repealing Directive 2006/66/EC. n.d. Available online: https://eur-lex.europa.eu/eli/reg/2023/1542/oj (accessed on 3 November 2024).
7. Song, S.-L.; Liu, R.-Q.; Sun, M.-M.; Zhen, A.-G.; Kong, F.-Z.; Yang, Y. Hydrometallurgical recovery of lithium carbonate and iron phosphate from blended cathode materials of spent lithium-ion battery. *Rare Met.* **2023**, *43*, 1275–1287. [CrossRef]
8. Dawkins, J.I.G.; Dawkins, J.I.G.; Pan, Y.; Pan, Y.; Ghavidel, M.Z.; Ghavidel, M.Z.; Geissler, J.; Geissler, J.; Krueger, B.; Krueger, B.; et al. Exploring the Synergistic Effects of Dual-Layer Electrodes for High Power Li-Ion Batteries. *ChemElectroChem* **2024**, *10*, e202300279. [CrossRef]
9. Julien, C.M.; Mauger, A.; Trottier, J.; Zaghib, K.; Hovington, P.; Groult, H. Olivine-based blended compounds as positive electrodes for lithium batteries. *Inorganics* **2016**, *4*, 17. [CrossRef]
10. Versaci, D.; Colombo, R.; Montinaro, G.; Buga, M.; Felix, N.C.; Evans, G.; Bella, F.; Amici, J.; Francia, C.; Bodoardo, S. Tailoring cathode materials: A comprehensive study on LNMO/LFP blending for next generation lithium-ion batteries. *J. Power Sources* **2024**, *613*, 234955. [CrossRef]
11. Kaur, G.; Gates, B.D. Review—Surface Coatings for Cathodes in Lithium Ion Batteries: From Crystal Structures to Electrochemical Performance. *J. Electrochem. Soc.* **2022**, *169*, 043504. [CrossRef]
12. Li, Y.; Zhao, P.; Shen, B. A review of new technologies for lithium-ion battery treatment. *Sci. Total. Environ.* **2024**, *951*, 175459. [CrossRef]
13. Zhao, Y.; Yuan, X.; Jiang, L.; Wen, J.; Wang, H.; Guan, R.; Zhang, J.; Zeng, G. Regeneration and reutilization of cathode materials from spent lithium-ion batteries. *Chem. Eng. J.* **2020**, *383*, 123089. [CrossRef]
14. Zhang, R.; Zheng, Y.; Yao, Z.; Vanaphuti, P.; Ma, X.; Bong, S.; Chen, M.; Liu, Y.; Cheng, F.; Yang, Z.; et al. Systematic Study of Al Impurity for NCM622 Cathode Materials. *ACS Sustain. Chem. Eng.* **2020**, *8*, 9875–9884. [CrossRef]
15. Ren, J.; Li, R.; Liu, Y.; Cheng, Y.; Mu, D.; Zheng, R.; Liu, J.; Dai, C. The impact of aluminum impurity on the regenerated lithium nickel cobalt manganese oxide cathode materials from spent LIBs. *New J. Chem.* **2017**, *41*, 10959–10965. [CrossRef]
16. Park, S.; Kim, D.; Ku, H.; Jo, M.; Kim, S.; Song, J.; Yu, J.; Kwon, K. The effect of Fe as an impurity element for sustainable resynthesis of $Li[Ni_{1/3}Co_{1/3}Mn_{1/3}]O_2$ cathode material from spent lithium-ion batteries. *Electrochim. Acta* **2019**, *296*, 814–822. [CrossRef]

17. Sa, Q.; Heelan, J.A.; Lu, Y.; Apelian, D.; Wang, Y. Copper Impurity Effects on $LiNi_{1/3}Mn_{1/3}Co_{1/3}O_2$ Cathode Material. *ACS Appl. Mater. Interfaces* **2015**, *7*, 20585–20590. [CrossRef] [PubMed]
18. Zhang, R.; Meng, Z.; Ma, X.; Chen, M.; Chen, B.; Zheng, Y.; Yao, Z.; Vanaphuti, P.; Bong, S.; Yang, Z.; et al. Understanding fundamental effects of Cu impurity in different forms for recovered $LiNi_{0.6}Co_{0.2}Mn_{0.2}O_2$ cathode materials. *Nano Energy* **2020**, *78*, 105214. [CrossRef]
19. Forte, F.; Pietrantonio, M.; Pucciarmati, S.; Puzone, M.; Fontana, D. Lithium iron phosphate batteries recycling: An assessment of current status. *Crit. Rev. Environ. Sci. Technol.* **2021**, *51*, 2232–2259. [CrossRef]
20. Li, H.; Xing, S.; Liu, Y.; Li, F.; Guo, H.; Kuang, G. Recovery of Lithium, Iron, and Phosphorus from Spent $LiFePO_4$ Batteries Using Stoichiometric Sulfuric Acid Leaching System. *ACS Sustain. Chem. Eng.* **2017**, *5*, 8017–8024. [CrossRef]
21. Ohnuma, T.; Kobayashi, T. X-ray absorption near edge structure simulation of $LiNi_{0.5}Co_{0.2}Mn_{0.3}O_2$*via* first-principles calculation. *RSC Adv.* **2019**, *9*, 35655–35661. [CrossRef]
22. Bzheumikhova, K.; Zech, C.; Schüler, K.; Vinson, J.; Kayser, Y.; Beckhoff, B. A multi-edge study: Investigating Co oxidation states of pristine $LiNi_xMn_yCo_{1-x-y}O_2$ cathode materials by high energy-resolution X-ray spectrometry. *Phys. Chem. Chem. Phys.* **2024**, *26*, 10599–10609. [CrossRef]
23. Billy, E.; Joulié, M.; Laucournet, R.; Boulineau, A.; De Vito, E.; Meyer, D. Dissolution Mechanisms of $LiNi_{1/3}Mn_{1/3}Co_{1/3}O_2$ Positive Electrode Material from Lithium-Ion Batteries in Acid Solution. *ACS Appl. Mater. Interfaces* **2018**, *10*, 16424–16435. [CrossRef]
24. Partinen, J.; Halli, P.; Wilson, B.P.; Lundström, M. The impact of chlorides on NMC leaching in hydrometallurgical battery recycling. *Miner. Eng.* **2023**, *202*, 108244. [CrossRef]
25. Jena, K.K.; AlFantazi, A.; Mayyas, A.T. Comprehensive Review on Concept and Recycling Evolution of Lithium-Ion Batteries (LIBs). *Energy Fuels* **2021**, *35*, 18257–18284. [CrossRef]
26. Zheng, R.; Wang, W.; Dai, Y.; Ma, Q.; Liu, Y.; Mu, D.; Li, R.; Ren, J.; Dai, C. A closed-loop process for recycling $LiNi_xCo_yMn_{(1-x-y)}O_2$ from mixed cathode materials of lithium-ion batteries. *Green Energy Environ.* **2017**, *2*, 42–50. [CrossRef]
27. Chen, X.; Li, J.; Kang, D.; Zhou, T.; Ma, H. A novel closed-loop process for the simultaneous recovery of valuable metals and iron from a mixed type of spent lithium-ion batteries. *Green Chem.* **2019**, *21*, 6342–6352. [CrossRef]
28. Zou, H.; Gratz, E.; Apelian, D.; Wang, Y. A novel method to recycle mixed cathode materials for lithium ion batteries. *Green Chem.* **2013**, *15*, 1183–1191. [CrossRef]
29. Xu, Z.; Dai, Y.; Hua, D.; Gu, H.; Wang, N. Creative Method for Efficiently Leaching Ni, Co, Mn, and Li in a Mixture of $LiFePO_4$ and $LiMO_2$ Using Only Fe(III). *ACS Sustain. Chem. Eng.* **2021**, *9*, 3979–3984. [CrossRef]
30. Zou, Y.; Chernyaev, A.; Ossama, M.; Seisko, S.; Lundström, M. Leaching of NMC industrial black mass in the presence of LFP. *Sci. Rep.* **2024**, *14*, 10818. [CrossRef]
31. Pagnanelli, F.; Altimari, P.; Schiavi, P.G.; D'Annibale, L.; Mancini, A.; Colasanti, M.; Moscardini, E.; Toro, L.; Baldassari, L.; Toro, L. LI-Ion battery recycling at pilot scale: Demonstrating the resynthesis route also for nmc-lfp mixed black mass. *Detritus* **2024**, *28*, 129–134. [CrossRef]
32. Illés, I.B.; Kékesi, T. Extraction of pure Co, Ni, Mn, and Fe compounds from spent Li-ion batteries by reductive leaching and combined oxidative precipitation in chloride media. *Miner. Eng.* **2023**, *201*, 108169. [CrossRef]
33. Jiang, Y.; Chen, X.; Yan, S.; Ou, Y.; Zhou, T. Mechanochemistry-induced recycling of spent lithium-ion batteries for synergistic treatment of mixed cathode powders. *Green Chem.* **2022**, *24*, 5987–5997. [CrossRef]
34. Pagnanelli, F.; Schiavi, P.G.; Altimari, P.; Beolchini, F.; Amato, A.; Coletta, J.; Forte, F.; Moscardini, E.; Toro, L. Economic and Environmental Sustainability of an Innovative Cryo-Mechano-Hydrometallurgical Process Validated at Pilot Scale for the Recycling of Li Batteries. *Metals* **2023**, *13*, 497. [CrossRef]
35. Commission Regulation (EU) No 493/2012 of 11 June 2012. Available online: https://eur-lex.europa.eu/legal-content/EN/TXT/HTML/?uri=CELEX:32012R0493&from=FI#d1e195-9-1 (accessed on 3 November 2024).
36. Winslow, K.M.; Laux, S.J.; Townsend, T.G. A review on the growing concern and potential management strategies of waste lithium-ion batteries. *Resour. Conserv. Recycl.* **2018**, *129*, 263–277. [CrossRef]
37. Granata, G.; Pagnanelli, F.; Moscardini, E.; Takacova, Z.; Havlik, T.; Toro, L. Simultaneous recycling of nickel metal hydride, lithium ion and primary lithium batteries: Accomplishment of European Guidelines by optimizing mechanical pre-treatment and solvent extraction operations. *J. Power Sources* **2012**, *212*, 205–211. [CrossRef]